

Quantum metric-induced oscillations in nearly dispersionless flat bands

Hui Zeng,^{1,2} Zijian Zhou,¹ Wenhui Duan,^{1,3,4,5} and Huaqing Huang^{2,5,6,*}

¹*State Key Laboratory of Low-Dimensional Quantum Physics,
Department of Physics, Tsinghua University, Beijing 100084, China*

²*School of Physics, Peking University, Beijing 100871, China*

³*Institute for Advanced Study, Tsinghua University, Beijing 100084, China*

⁴*Frontier Science Center for Quantum Information, Beijing 100084, China*

⁵*Collaborative Innovation Center of Quantum Matter, Beijing 100871, China*

⁶*Center for High Energy Physics, Peking University, Beijing 100871, China*

(Dated: March 26, 2025)

Abstract

The transport of Bloch electrons under strong fields is traditionally understood through two mechanisms: intraband Bloch oscillations and interband Zener tunneling. Here we propose a new oscillation mechanism induced by the interband quantum metric, which would significantly affect the electron dynamics under strong fields. By considering the multiband dynamics to the second order of the density matrix, we reveal that quantum metric-induced oscillations (QMO) persist regardless of band dispersion, even in exactly dispersionless flat bands. The resultant drift current can reach a magnitude comparable to the Bloch oscillation-induced drift current in systems where interband tunneling is negligible. Notably, the QMO-induced drift current increases linearly with electric field strength under the constraints of time-reversal or spatial-inversion symmetry, emerging as the primary delocalized current. We further show that both one-dimensional and two-dimensional superlattices are potential platforms for investigating QMO.

Introduction.—The strong-field dynamics of Bloch electrons has been an important area of research in condensed matter physics for decades. Among the well-known phenomena are Bloch oscillations (BO) [1], arising from band dispersion, and interband Zener tunneling (ZT) [2], particularly near anti-crossing points. While oscillations reflect the intrinsic periodicity of the system, interband tunneling disrupts these oscillations. BO induces Wannier-Stark localization, with a steady drift current that decreases as the electric field increases, while ZT causes delocalization, resulting in a steady current that increases with the field. Extensive studies have explored these phenomena in one-dimensional (1D) superlattices, from strong-field transport in solids [3–9] to optical [10–14] and cold-atom [15, 16] simulations. Recent breakthroughs in fabricating two-dimensional (2D) moiré superlattices featuring flat minibands [17] have reignited interest in strong-field transport [18–20]. Furthermore, oscillations arising from the anomalous velocity induced by Berry curvature (i.e., Berry curvature-induced oscillations, BCO) [21, 22] has emerged as another significant mechanism influencing strong-field responses in 2D flat-band solids. This highlights the non-negligible role of quantum geometry in understanding the behavior of materials under strong fields.

Non-interacting, nearly dispersionless bands without anti-crossing points, referred to as flat bands in this work, are commonly considered ideal platforms for observing intraband oscillations, i.e., BO [18, 23] and BCO [21, 22]. This is because interband ZT typically occurs

near anti-crossing points where energy bands approach one another [20, 21, 23–27]. However, previous experiments have detected substantial delocalized current in GaAs/Al_xGa_{1-x}As superlattices, a flat-band system where tunneling is negligible [7], suggesting the need for a mechanism beyond the conventional BO-ZT framework. In this work, we demonstrate that interband coherence driven by the quantum metric can significantly affect strong-field transport, emerging as a key contributor to delocalized currents in flat bands. This highlights the necessity of a deeper investigation into interband quantum geometric effects.

In this Letter, we reveal a new type of oscillation driven by the interband quantum metric which characterizes the distance of Bloch states between different bands. We show that the quantum metric-induced oscillations (QMO) occur even in exactly flat bands where conventional BO vanishes. Remarkably, the delocalized drift current from QMO exhibits a linear growth asymptotic behavior in the strong-field regime, which is distinct from the BO-induced localized drift current decaying as E^{-1} or the BCO-induced drift current saturating to an E -independent value. Notably, the QMO-induced drift current in flat-band systems can reach a magnitude comparable to the BO-induced drift current when the system is far from ZT-induced breakdown, thus representing a significant mechanism beyond interband tunneling that resists the BO-induced localization. Furthermore, we show that both 1D and 2D superlattices are potential platforms for investigating the QMO.

Recursive formula for strong-field transports.—We start by establishing the recursive formula of the density matrix to address the multi-band-coupled strong field problems, which requires a derivation beyond the standard weak-field expansion [28–35]. To study the electronic response properties under an external electric field, we begin with the master equation in the relaxation-time approximation [36]:

$$i\hbar\partial_t\rho = [H_0 + H_1, \rho] - i(\rho - \rho^0)\hbar/\tau, \quad (1)$$

where $\rho(\mathbf{k}, t)$ is the density matrix operator in momentum space, and hereafter we omit the explicit dependence of \mathbf{k} for brevity, unless otherwise specified. $\rho^0 = f_n^0\delta_{nm}$ is the equilibrium Fermi-Dirac distribution, and we assume zero temperature unless otherwise specified. H_0 is the Hamiltonian without an external field, τ is the relaxation time, and $H_1 = e\mathbf{E}\cdot\mathbf{r}$ captures the coupling between the external electric field and electron. The position operator in the Bloch basis is represented as $[\mathbf{r}_{\mathbf{k}}]_{nm} = i\partial_{\mathbf{k}}\delta_{nm} + \mathcal{A}_{nm}$, where \mathcal{A} is the Berry connection.

It should be noted that four energy scales appear in Eq. (1): the characteristic frequency

$\hbar\omega$ ($i\hbar\partial_t$) of the density matrix evolution; the energy gap $\epsilon_{nm} = \epsilon_n - \epsilon_m$ from the eigenvalues of H_0 ; the external field strength characterized by eEa from H_1 with a the lattice constant; and the relaxation process characterized by \hbar/τ . In this work, we consider the large-gap condition, i.e., $\epsilon_{nm} \gg \max\{\hbar\omega, eEa, \hbar/\tau\}$, which includes two more specific cases. One is characterized by a weak field ($\epsilon_{nm} \gg \hbar/\tau \gg eEa$) where various weak-field response properties can be obtained [28–35, 37–40]. The other condition pertains to a strong field under the large-gap presupposition ($\epsilon_{nm} \gg eEa \gg \hbar/\tau$). This refined energy scale condition, which is our main concern, would dedicate fascinating situations where $\hbar\omega \neq 0$ leads to oscillatory currents, while $\hbar\omega = 0$ corresponds to drift currents, as we discussed later.

Considering the time scale of BO ($\omega \sim eEa/\hbar$) and steady transports, we expand Eq. (1) under the large-gap condition. This leads us to a recursive formula for the off-diagonal and diagonal terms of the density matrix $\rho(t)$:

$$\begin{aligned} \epsilon_{nm}\rho_{nm}^{(N)}(t) = & -e\mathbf{E} \cdot [\mathcal{A}, \rho^{(N-1)}(t)]_{nm} \\ & -i(e\mathbf{E} \cdot \partial_{\mathbf{k}} - \hbar\partial_t - \hbar/\tau)\rho_{nm}^{(N-1)}(t), \end{aligned} \quad (2)$$

$$\begin{aligned} 0 = & -e\mathbf{E} \cdot [\mathcal{A}, \rho^{(N)}(t)]_{nn} \\ & -i(e\mathbf{E} \cdot \partial_{\mathbf{k}} - \hbar\partial_t - \hbar/\tau)\rho_{nn}^{(N)}(t), \end{aligned} \quad (3)$$

where $\rho^{(N)}$ represents the N -th order term of $1/\epsilon_{nm}$, $[\mathcal{A}, \rho^{(N)}(t)]_{nm} = \sum_p (\mathcal{A}_{np}\rho_{pm}^{(N)} - \rho_{np}^{(N)}\mathcal{A}_{pm})$. These formulas apply to both weak-field and strong-field cases, as shown in Supplementary Materials (SM) [36]. Furthermore, we introduce the diagonal density matrix $\rho^{(0)}$, which satisfies the master equation Eq. (1) at the zeroth order, as the starting point for the recursive process

$$\rho_{s,nm}^{(0)} = \sum_{\mathbf{a}_i} \frac{f_{n,\mathbf{a}_i}^0 e^{i\mathbf{k}\cdot\mathbf{a}_i}}{1 - i\tau e\mathbf{E} \cdot \mathbf{a}_i/\hbar} \delta_{nm}, \quad t \gg \tau \quad (4)$$

$$\rho_{nm}^{(0)}(\mathbf{k}, t) = \rho_{nm}(\mathbf{k} + e\mathbf{E}t/\hbar, 0)\delta_{nm}, \quad t \ll \tau \quad (5)$$

where f_{n,\mathbf{a}_i}^0 is \mathbf{a}_i Fourier component of Fermi-Dirac distribution. $\rho_s^{(0)}$ is the zeroth order density matrix for the steady state after full relaxation [21], and $\rho^{(0)}(\mathbf{k}, t)$ represents the zeroth order density matrix for the non-steady oscillating state far from complete relaxation. Note that under the large gap condition, the small quantity is $1/\epsilon_{nm}$ instead of E . E is allowed to appear in $\rho^{(0)}$, capturing the non-perturbative effects of a strong electric field on the momentum-space electron distribution.

Having obtained the density matrix, we can derive the electric current $\mathbf{J} = -e \text{Tr}[\rho \mathbf{v}]$, where the velocity operator can be expressed in the Bloch basis as $[\mathbf{v}]_{nm} = \frac{1}{\hbar}(\partial_{\mathbf{k}} \epsilon_n \delta_{nm} + i \epsilon_{nm} \mathcal{A}_{nm})$. The $\omega = 0$ steady component of the *zeroth-order* and *first-order* density matrix respectively give the BO and BCO induced drift currents [21] in 2D under the strong-field condition

$$\mathbf{J}_{\text{Bloch}} = -\frac{e}{\hbar} \int_{\text{BZ}} [d\mathbf{k}] \sum_n \rho_{s,nn}^{(0)} \nabla_{\mathbf{k}} \epsilon_n, \quad (6)$$

$$\mathbf{J}_{\Omega} = -\frac{e}{\hbar} \int_{\text{BZ}} [d\mathbf{k}] \sum_n \rho_{s,nn}^{(0)} e \mathbf{E} \times \Omega_n, \quad (7)$$

where the integral is over the 2D Brillouin zone (BZ) with $[d\mathbf{k}] \equiv d^2k/(2\pi)^2$, Berry curvature $\Omega_n = 2 \sum_m \text{Im}(\mathcal{A}_{nm}^x \mathcal{A}_{mn}^y)$. Correspondingly, we can also obtain the BO and BCO oscillatory currents, which share similar expressions as Eqs. (6) and (7) only with $\rho_s^{(0)}$ replaced by $\rho^{(0)}(t)$. These expressions of BO and BCO are consistent with those derived from the semiclassical wave packet dynamics for a single band [21]. Moreover, our recursive formula allows us to comprehensively address both intraband and interband effects simultaneously.

QMO-induced Drift current.—Now, we take a step further to consider the *second-order* density matrix of steady state, which results in drift current induced by QMO (\mathbf{J}_g) and ZT (\mathbf{J}_{ZT}). Specifically, \mathbf{J}_g and \mathbf{J}_{ZT} are determined by the second-order off-diagonal and diagonal terms of the density matrix, derived from Eqs. (2) and (3), respectively. Although \mathbf{J}_{ZT} is much smaller than \mathbf{J}_g in flat-band systems, as illustrated later, here we introduce both for the sake of completeness,

$$\begin{aligned} \mathbf{J}_g^a = & -\frac{e^2 E^c}{\hbar} \int_{\text{BZ}} [d\mathbf{k}] \sum_{n,m \neq n} \rho_{s,nn}^{(0)} \frac{2g_{nm}^{ac} \hbar/\tau}{\epsilon_{nm}} \\ & -\frac{e^3 E^b E^c}{\hbar} \int_{\text{BZ}} [d\mathbf{k}] \sum_{n,m \neq n} \left[\rho_{s,nn}^{(0)} \frac{(\partial_a g_{nm}^{bc})}{\epsilon_{nm}} \right], \end{aligned} \quad (8)$$

$$\mathbf{J}_{\text{ZT}}^a = -\frac{e}{\hbar} \int_{\text{BZ}} [d\mathbf{k}] \sum_n [\rho_{nn}^{(2)} \nabla_a \epsilon_n], \quad (9)$$

$$\begin{aligned} \rho_{nn}^{(2)} = & \sum_{\mathbf{a}_i} \frac{e^{i\mathbf{k} \cdot \mathbf{a}_i}}{e \mathbf{E} \cdot \mathbf{a}_i + i\hbar/\tau} \sum_{m \neq n} \left[e^2 E^d E^c \frac{i\hbar}{\tau} 2g_{nm}^{dc} \frac{\rho_{s,nn}^{(0)}}{\epsilon_{nm}^2} \right. \\ & + \frac{i e^3 E^d E^b E^c}{\epsilon_{nm}} \left((\partial_b g_{nm}^{dc}) \frac{\rho_{s,nn}^{(0)}}{\epsilon_{nm}} + 2g_{nm}^{dc} \partial_b \left(\frac{\rho_{s,nn}^{(0)}}{\epsilon_{nm}} \right) \right) \\ & \left. - (n \leftrightarrow m) \right]_{\mathbf{a}_i}, \end{aligned} \quad (10)$$

where a, b, c are Cartesian indices (Einstein summation convention assumed), $[\cdot]_{\mathbf{a}_i}$ denotes

the \mathbf{a}_i Fourier component, and $g_{nm}^{ab} = \text{Re}(\mathcal{A}_{nm}^a \mathcal{A}_{mn}^b)$ is the quantum metric. Unlike BCO-induced drift current \mathbf{J}_Ω , which has only a transverse component and vanishes in 1D systems [21], \mathbf{J}_g has both longitudinal and transverse components, making it detectable in both 1D and higher-dimensional systems.

Notably, in systems with symmetry of time reversal (\mathcal{T}) or space inversion (\mathcal{P}), \mathbf{J}_g is proportional to E asymptotically, although Eq. (8) appears to include E^2 terms. This is because the fluctuations of $\rho_{s,nn}^{(0)}$ are always suppressed by factor $1/(e\mathbf{E} \cdot \mathbf{a}_i)$, as shown in Eq. (4). In the second term of \mathbf{J}_g (Eq. (8)), \mathcal{T} or \mathcal{P} symmetry constrains g_{nm} and ϵ_{nm} to be even to \mathbf{k} , which in turn requires that only the \mathbf{k} -odd fluctuations of $\rho_{s,nn}^{(0)}$ contribute to the integration. Therefore, both terms in Eq. (8) are linear to E . The same symmetry constraint also applies to \mathbf{J}_{ZT} , and an additional $1/(e\mathbf{E} \cdot \mathbf{a}_i)$ factor is introduced for $\rho_{s,nn}^{(2)}$, as shown in Eq. (10). This leads to \mathbf{J}_{ZT} also being proportional to E . More detailed discussions about the asymptotical behaviors under symmetry constraints are presented in SM [36].

We first illustrate the drift currents in a 1D GaAs/Al_xGa_{1-x}As superlattice, which was usually used to study the BO [3–9]. We adopt a 1D effective model to describe the two bottom conduction minibands of the superlattice composed of alternating GaAs and Al_{0.3}Ga_{0.7}As layers with width $u = 95 \text{ \AA}$ and $l = 25 \text{ \AA}$ [9], as shown in Fig. 1(a). The specifics of these calculations are detailed in SM [36]. Figure 1(b) shows the calculated band structure and quantum metric, where the bandwidths are $W_{0,1} = 10$ and 40 meV and the energy gap between them is $\Delta = 70 \text{ meV}$. Taking a typical relaxation time $\tau \simeq 0.13 \text{ ps}$, which satisfies the large-gap approximation (i.e., $\hbar/\tau = \Delta/14 \ll \Delta$), we calculate the zeroth order lower band occupation $\rho_{s,00}^{(0)}$ and ZT-induced conduction band occupation $\rho_{s,11}^{(2)} = -\rho_{s,00}^{(2)}$ in the presence of an external field of $E = \Delta/2ea$. As shown in Fig. 1(c), the negligible $\rho_{s,11}^{(2)} (\ll 1)$ ensures the system is far away from the breakdown, which indicates a small tunneling current $J_{\text{ZT}} (\ll J_{\text{Bloch}}, J_g)$ [see Fig. 1(d)].

Importantly, we find a considerable drift current J_g , which is comparable to J_{Bloch} , as shown in Figs. 1(e,f). Moreover, J_g increases linearly under large electric fields, while J_{Bloch} decays with the increasing E . This indicates that in flat-band systems, contrary to the traditional view that ZT is the primary mechanism for delocalized current, \mathbf{J}_g is actually the main source of such current. Previous research in 1D superlattices has observed a transition from localized current with negative differential resistance to delocalized current, with ZT being negligible [7]. We suggest that \mathbf{J}_g should be considered an important source of

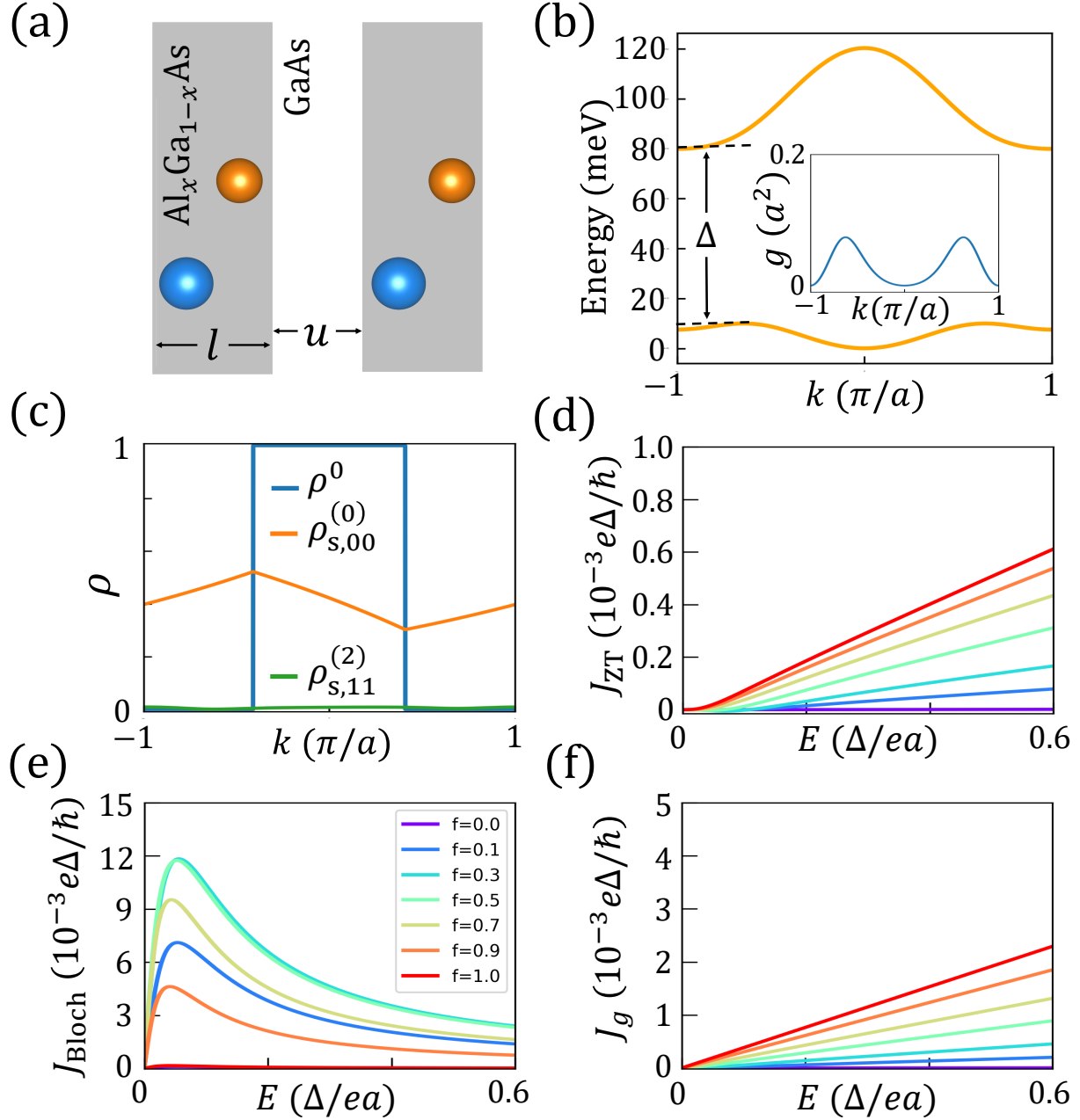


FIG. 1. Drift currents in GaAs/ $\text{Al}_x\text{Ga}_{1-x}\text{As}$ superlattices. (a) Sketch of an effective 1D model with two orbitals for the two bottom conduction bands of the superlattice. (b) Band structure and quantum metric of the 1D model. (c) Equilibrium (Fermi-Dirac) filling distribution ρ^0 at band filling $f = 0.4$, zeroth order distribution $\rho_{00}^{(0)}$ under a strong field of $E = \Delta/2ea$, and ZT-induced upper band occupation $\rho_{11}^{(2)} = -\rho_{00}^{(2)}$. (d-f) J_{ZT} , J_{Bloch} and J_g as functions of field strength E for the lower band with different fillings [denoted as f in (e)].

the delocalized current. Additionally, unlike J_{Bloch} which reaches the maximum in half-filled bands but vanishes in fully-filled bands, J_g increases with the filling factor, highlighting its origin in interband coupling.

We further study the QMO-induced drift current \mathbf{J}_g in a 2D honeycomb lattice model [36], which has been suggested as a good platform for studying $\mathbf{J}_{\text{Bloch}}$ [18] and \mathbf{J}_Ω [21, 22]. Here, we only present two dominant longitudinal currents J_{Bloch}^L and J_g^L , and defer detailed discussion about small \mathbf{J}_{ZT} and transverse currents to SM [36]. Figures 2(a,b) display the valence band energy E_v and the g_{xx} component of the quantum metric, which are the origins of J_{Bloch}^L and J_g^L , respectively, when the electric field E is directed along the x -axis. The nontrivial E_v and g_{xx} induce J_{Bloch}^L and J_g^L , which exhibit inverse decay and linear increase with E , respectively, as shown in Figs. 2(c,d). The magnitudes of J_{Bloch} and J_g are comparable. Moreover, J_{Bloch} shows a hexagonal dependence on the electric field direction, while J_g exhibits an isotropic asymptotic behavior, as displayed in Figs. 2(e,f). These features indicate that J_g constitutes a significant delocalized current in 2D systems.

Quantum metric-induced oscillations.—Next, we turn to time-dependent cases to study the quantum metric-induced oscillatory current. Specifically, we consider the time evolution of both the diagonal $\rho_{nn}^{(0)}(k, t)$ and off-diagonal $\rho_{nm}^{(0)}(k, t)$ density matrices from arbitrary initial states, which leads to oscillations at low and high frequencies (i.e., BO and ϵ_{nm} frequency), respectively. Given that the recursive formula Eq. (2) holds for both steady ($\omega = 0$) and oscillatory ($\omega \sim eEa/\hbar$) states, the QMO-induced oscillatory current $J_g(t)$ at BO frequency can be obtained by simply replacing $1/\tau$ and $\rho_s^{(0)}$ in Eq. (8) with $i\omega$ and $\rho_{nm}^{(0)}(\omega)$. In particular, $J_g(t)$ in 1D systems can be expressed as [36],

$$J_{g,\text{BO-freq}}(t) = -\frac{e^2 E}{\hbar} \int \frac{dk}{2\pi} \sum_{n,m \neq n} \partial_t \rho_{nm}^{(0)}(k, t) \frac{g_{nm}}{\epsilon_{nm}}. \quad (11)$$

Alternatively, a high-frequency oscillatory current arises from the off-diagonal density matrices, whose zeroth order term in flat bands is $\rho_{nm}^{(0)}(k, t) = \rho_{nm}(k + eEt/\hbar, 0)e^{-i\epsilon_{nm}t/\hbar}$ and higher-order low-frequency modulation can be derived with recursive formulas under the large-gap approximation (see SM [36] for detailed discussions). Specifically, for a 1D state starting with density matrix with off-diagonal component $\rho_{nm}(k, 0)$, its time-evolution is characterized by $\rho_{nm}(k, t) = e^{-i\epsilon_{nm}t/\hbar} C_{nm}(k, t) \mathcal{A}_{nm}(k)$, where $C_{nm}(k, t)$ determined by $\rho_{nm}(k + eEt/\hbar, 0) = C_{nm}(k, t) \mathcal{A}_{nm}(k)$ oscillates with a period equal to that of Bloch oscillations. The ϵ_{nm} -frequency component of the QMO-induced oscillatory current $J_g(t)$ is given

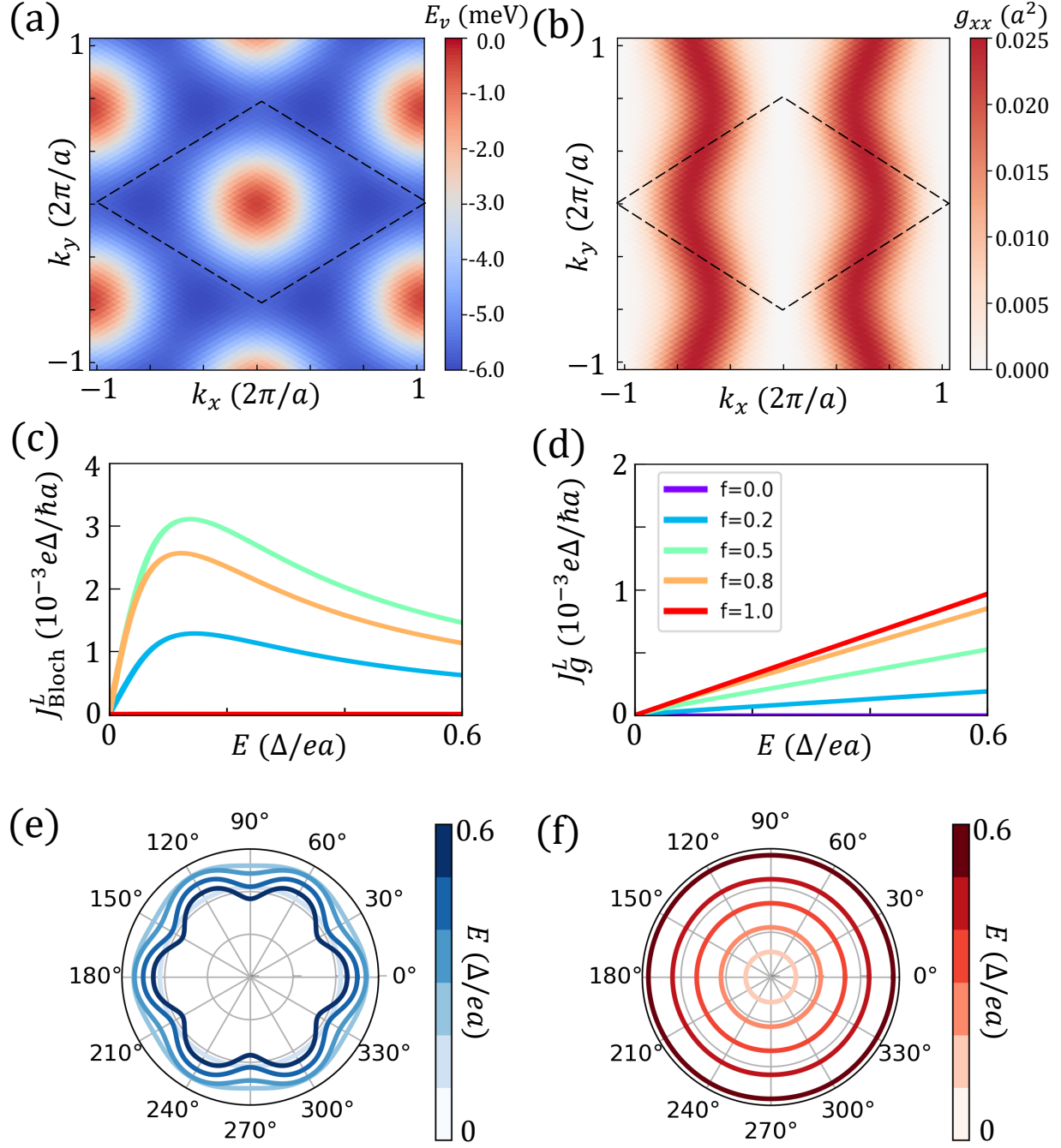


FIG. 2. Bloch and quantum metric induced drift currents in 2D honeycomb lattice. (a) Valence band E_v and (b) g_{xx} component of quantum metric in the 2D honeycomb lattice model. (c,d) show the longitudinal component of J_{Bloch} and J_g varying with external electric field E directed in x when valence band has different fillings. (e,f) show how J_{Bloch} and J_g vary with electric field directions and field strengths, at a filling of 0.6.

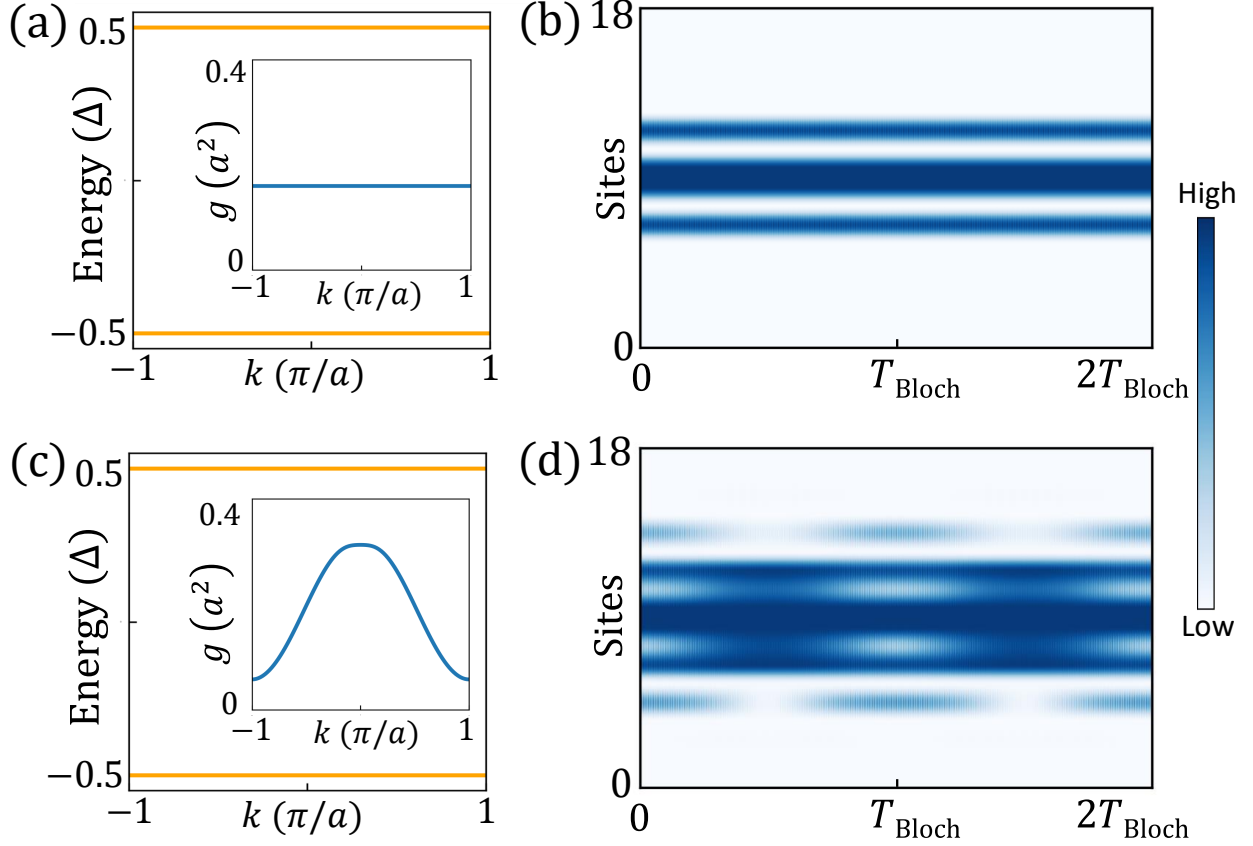


FIG. 3. Quantum metric-induced oscillations lead to breathing modes of probability density in 1D lattice model with 18 sites. (a,b) Model with exactly flat bands and constant quantum metric g do not exhibit any oscillations. (c,d) When a non-constant quantum metric is introduced into the exactly flat bands, QMO-induced breathing mode emerges, and probability density evolves periodically in time. Two orbitals are shown on two sites separately.

by

$$J_{g,\epsilon\text{-freq}}(t) = \frac{e}{\hbar} \int \frac{dk}{2\pi} \sum_{n,m \neq n} \text{Im} \left(e^{-i\epsilon_{nm}t/\hbar} C_{nm}(k,t) \right) \epsilon_{nm} g_{nm}. \quad (12)$$

Although it does not generate a net current on the BO time scale, as the high-frequency current is averaged out, it can dominate the breathing mode produced by the evolution of wave packets on the lattice.

Notably, J_g occurs even in exactly flat bands when g varies in momentum space, but vanishes if both ϵ_{nm} and g_{nm} are constant. This is because both $\rho_{nn}^{(0)}(k,t) = \rho_{nn}(k + eEt/\hbar, 0)$ and $\rho_{nm}(k,t) = \rho_{nm}(k + eEt/\hbar, 0)$ are just shifting within the Brillouin zone, and therefore, when ϵ_{nm} and g_{nm} are constant, the integrals in Eqs. (11) and (12) do not change in BO time

scale. However, when g varies, it imparts a non-constant weight to the integrals, causing the integral results periodically evolve at the Bloch frequency. In addition, the amplitudes of $J_{g,\text{BO-freq}}(t)$ and $J_{g,\epsilon\text{-freq}}(t)$ do not decay with increasing electric field [36]. This characteristic distinguishes them from BO and provides potential probes of the quantum metric in periodic systems.

1D lattices are excellent platforms for studying BO [10–16] and can also be used to investigate QMO. The periodic evolution of the wavepacket probability distribution over the lattice, known as the breathing mode, visualizes the oscillatory behavior. To directly illustrate QMO, we numerically simulate the time-dependent evolution of a wave packet in a 1D two-band model with exactly flat bands, where BO vanishes due to the absence of band dispersion. The model’s Hamiltonian is given by $H = \mathbf{h}(k) \cdot \boldsymbol{\sigma}$, with $\boldsymbol{\sigma}$ the Pauli matrix. An exactly flat band structure can be achieved by setting $|\mathbf{h}| = m$ as a constant. The quantum metric g can be tuned by the normalized vector $\mathbf{n}(k) = \mathbf{h}(k)/|\mathbf{h}|$. We place the model on a lattice with 9 unit-cells (18 sites). When $h_x = t \cos(ka)$, $h_y = t \sin(ka)$, g is also flat, and no QMO occurs, thus no breathing mode appears, as shown in Figs. 3(a,b). However, if we set $h_x = t \cos(ka) + t' \cos(2ka)$, $h_y = t \sin(ka) + t' \sin(2ka)$, which can be approximated with several short-range hopping terms [36], g fluctuates in momentum space, leading to oscillatory behaviors in the time evolution of the real-space probability density, as illustrated in Figs. 3(c,d). This demonstrates that even in exactly flat bands where BO vanishes, QMO can still survive. We also checked the consistency between numerical simulations and analytical calculations [36].

Discussion and summary— Our proposed QMO is expected to be experimentally observed in various platforms, especially the solid superlattices with flat bands that have been used to study BO. For instance, in 1D epitaxial superlattices where various signals caused by BO have been detected [3–8], flat bands can be engineered such that ZT-induced current is neglectable, BO-induced current dominates at weak fields near half-filling, and QMO-induced current dominates under strong fields when the system is away from breakdown. 2D moiré superlattices are also promising platforms, as their tunable band structures and rich quantum geometry would facilitate the observation of both BO- [18] and BCO [21, 22]-induced drift currents. We discuss feasible experiments with more details in SM [36]. Moreover, various artificial periodic systems, including optical [10–14] and cold atom lattices [15, 16], where BO has been extensively studied, offer potential platforms for ob-

serving the oscillatory behaviors of QMO and merit further exploration. As a mechanism generally present in periodic systems, QMO opens up new opportunities for studying quantum metrics in these systems.

In summary, we reveal a strong-field oscillation mechanism induced by interband quantum metric, which can manifest even in exactly flat bands. The QMO-induced drift current in a steady state exhibits a linear dependence on the electric field in \mathcal{T} - or \mathcal{P} -symmetric systems, emerging as the dominant delocalized current in flat bands. In addition, signals arising from QMO hold promise for detection in systems with flat bands, including 1D epitaxial superlattices and 2D moiré lattices.

This work is supported by the National Key R&D Program of China (Grant No. 2021YFA1401600), the National Natural Science Foundation of China (Grants No. 12074006 and 12474056), the Basic Science Center Project of NSFC (Grant No. 52388201), the Ministry of Science and Technology of China, and the Beijing Advanced Innovation Center for Future Chip (ICFC). The computational resources were supported by the high-performance computing platform of Peking University.

* Corresponding author: huaqing.huang@pku.edu.cn

- [1] F. Bloch, Quantum mechanics of electrons in crystal lattices, *Z. Phys* **52**, 555 (1928).
- [2] C. Zener, A theory of the electrical breakdown of solid dielectrics, *Proceedings of the Royal Society of London. Series A, Containing Papers of a Mathematical and Physical Character* **145**, 523 (1934).
- [3] K. Leo, P. H. Bolivar, F. Brüggemann, R. Schwedler, and K. Köhler, Observation of bloch oscillations in a semiconductor superlattice, *Solid State Commun.* **84**, 943 (1992).
- [4] J. Feldmann, K. Leo, J. Shah, D. A. B. Miller, J. E. Cunningham, T. Meier, G. von Plessen, A. Schulze, P. Thomas, and S. Schmitt-Rink, Optical investigation of bloch oscillations in a semiconductor superlattice, *Phys. Rev. B* **46**, 7252 (1992).
- [5] C. Waschke, H. G. Roskos, R. Schwedler, K. Leo, H. Kurz, and K. Köhler, Coherent submillimeter-wave emission from bloch oscillations in a semiconductor superlattice, *Phys. Rev. Lett.* **70**, 3319 (1993).
- [6] A. Sibille, J. F. Palmier, H. Wang, and F. Mollot, Observation of esaki-tsu negative differential

- velocity in gaas/alas superlattices, Phys. Rev. Lett. **64**, 52 (1990).
- [7] F. Beltram, F. Capasso, D. L. Sivco, A. L. Hutchinson, S.-N. G. Chu, and A. Y. Cho, Scattering-controlled transmission resonances and negative differential conductance by field-induced localization in superlattices, Phys. Rev. Lett. **64**, 3167 (1990).
- [8] T. Dekorsy, R. Ott, H. Kurz, and K. Köhler, Bloch oscillations at room temperature, Phys. Rev. B **51**, 17275 (1995).
- [9] A. M. Bouchard and M. Luban, Bloch oscillations and other dynamical phenomena of electrons in semiconductor superlattices, Phys. Rev. B **52**, 5105 (1995).
- [10] H. Trompeter, T. Pertsch, F. Lederer, D. Michaelis, U. Streppel, A. Bräuer, and U. Peschel, Visual observation of zener tunneling, Phys. Rev. Lett. **96**, 023901 (2006).
- [11] F. Dreisow, A. Szameit, M. Heinrich, T. Pertsch, S. Nolte, A. Tünnermann, and S. Longhi, Bloch-zener oscillations in binary superlattices, Phys. Rev. Lett. **102**, 076802 (2009).
- [12] S. Longhi, Bloch oscillations in complex crystals with \mathcal{PT} symmetry, Phys. Rev. Lett. **103**, 123601 (2009).
- [13] R. Sapienza, P. Costantino, D. Wiersma, M. Ghulinyan, C. J. Oton, and L. Pavesi, Optical analogue of electronic bloch oscillations, Phys. Rev. Lett. **91**, 263902 (2003).
- [14] R. Morandotti, U. Peschel, J. S. Aitchison, H. S. Eisenberg, and Y. Silberberg, Experimental observation of linear and nonlinear optical bloch oscillations, Phys. Rev. Lett. **83**, 4756 (1999).
- [15] O. Morsch, J. H. Müller, M. Cristiani, D. Ciampini, and E. Arimondo, Bloch oscillations and mean-field effects of bose-einstein condensates in 1d optical lattices, Phys. Rev. Lett. **87**, 140402 (2001).
- [16] M. Ben Dahan, E. Peik, J. Reichel, Y. Castin, and C. Salomon, Bloch oscillations of atoms in an optical potential, Phys. Rev. Lett. **76**, 4508 (1996).
- [17] C. N. Lau, M. W. Bockrath, K. F. Mak, and F. Zhang, Reproducibility in the fabrication and physics of moiré materials, Nature **602**, 41 (2022).
- [18] A. Fahimniya, Z. Dong, E. I. Kiselev, and L. Levitov, Synchronizing bloch-oscillating free carriers in moiré flat bands, Phys. Rev. Lett. **126**, 256803 (2021).
- [19] T. Vakhtel, D. O. Oriekhov, and C. W. J. Beenakker, Bloch oscillations in the magnetoconductance of twisted bilayer graphene, Phys. Rev. B **105**, L241408 (2022).
- [20] L.-L. Ye and Y.-C. Lai, Irregular bloch-zener oscillations in two-dimensional flat-band dirac materials, Phys. Rev. B **107**, 165422 (2023).

- [21] V. o. T. Phong and E. J. Mele, Quantum geometric oscillations in two-dimensional flat-band solids, *Phys. Rev. Lett.* **130**, 266601 (2023).
- [22] C. De Beule and E. J. Mele, Berry curvature spectroscopy from bloch oscillations, *Phys. Rev. Lett.* **131**, 196603 (2023).
- [23] J. M. Pruneda and I. Souza, Nonadiabatic wavepacket dynamics: k -space formulation, *Phys. Rev. B* **79**, 045127 (2009).
- [24] B. Rosam, D. Meinhold, F. Löser, V. G. Lyssenko, S. Glutsch, F. Bechstedt, F. Rossi, K. Köhler, and K. Leo, Field-induced delocalization and zener breakdown in semiconductor superlattices, *Phys. Rev. Lett.* **86**, 1307 (2001).
- [25] R. Khomeriki and S. Flach, Landau-zener bloch oscillations with perturbed flat bands, *Phys. Rev. Lett.* **116**, 245301 (2016).
- [26] S. Kitamura, N. Nagaosa, and T. Morimoto, Nonreciprocal landau–zener tunneling, *Communications Physics* **3**, 1 (2019).
- [27] S. Kitamura, N. Nagaosa, and T. Morimoto, Current response of nonequilibrium steady states in the landau-zener problem: Nonequilibrium green’s function approach, *Phys. Rev. B* **102**, 245141 (2020).
- [28] Y. Gao, S. A. Yang, and Q. Niu, Field induced positional shift of bloch electrons and its dynamical implications, *Phys. Rev. Lett.* **112**, 166601 (2014).
- [29] C. Wang, Y. Gao, and D. Xiao, Intrinsic nonlinear hall effect in antiferromagnetic tetragonal cumnas, *Phys. Rev. Lett.* **127**, 277201 (2021).
- [30] H. Liu, J. Zhao, Y.-X. Huang, W. Wu, X.-L. Sheng, C. Xiao, and S. A. Yang, Intrinsic second-order anomalous hall effect and its application in compensated antiferromagnets, *Phys. Rev. Lett.* **127**, 277202 (2021).
- [31] J. Wang, H. Zeng, W. Duan, and H. Huang, Intrinsic nonlinear hall detection of the néel vector for two-dimensional antiferromagnetic spintronics, *Phys. Rev. Lett.* **131**, 056401 (2023).
- [32] A. Gao, Y.-F. Liu, J.-X. Qiu, B. Ghosh, T. V. Trevisan, Y. Onishi, C. Hu, T. Qian, H.-J. Tien, S.-W. Chen, M. Huang, D. Bérubé, H. Li, C. Tzschaschel, T. Dinh, Z. Sun, S.-C. Ho, S.-W. Lien, B. Singh, K. Watanabe, T. Taniguchi, D. C. Bell, H. Lin, T.-R. Chang, C. R. Du, A. Bansil, L. Fu, N. Ni, P. P. Orth, Q. Ma, and S.-Y. Xu, Quantum metric nonlinear hall effect in a topological antiferromagnetic heterostructure, *Science* **381**, 181 (2023).
- [33] D. Kaplan, T. Holder, and B. Yan, Unification of nonlinear anomalous hall effect and nonre-

- reciprocal magnetoresistance in metals by the quantum geometry, *Phys. Rev. Lett.* **132**, 026301 (2024).
- [34] K. Das, S. Lahiri, R. B. Atencia, D. Culcer, and A. Agarwal, Intrinsic nonlinear conductivities induced by the quantum metric, *Phys. Rev. B* **108**, L201405 (2023).
- [35] N. Wang, D. Kaplan, Z.-G. Zhang, T. Holder, N. Cao, A. Wang, X. Zhou, F. Zhou, Z. Jiang, C. Zhang, S. Ru, H. Cai, K. Watanabe, T. Taniguchi, B. Yan, and W. Gao, Quantum-metric-induced nonlinear transport in a topological antiferromagnet, *Nature* **621**, 487 (2023).
- [36] See Supplemental Material at <http://link.aps.org/supplemental/xxx>, for more details about the approximations, derivations of the drift & oscillatory currents, numerical calculations, and possible experimental realizations. Refs. [3–7, 10–22, 26–35, 38, 41–68] are included.
- [37] N. Nagaosa, J. Sinova, S. Onoda, A. H. MacDonald, and N. P. Ong, Anomalous hall effect, *Rev. Mod. Phys.* **82**, 1539 (2010).
- [38] I. Sodemann and L. Fu, Quantum nonlinear hall effect induced by berry curvature dipole in time-reversal invariant materials, *Phys. Rev. Lett.* **115**, 216806 (2015).
- [39] Q. Ma, S.-Y. Xu, H. Shen, D. MacNeill, V. Fatemi, T.-R. Chang, A. M. M. Valdivia, S. Wu, Z. Du, C. Hsu, S. Fang, Q. D. Gibson, K. Watanabe, T. Taniguchi, R. J. Cava, E. Kaxiras, H.-Z. Lu, H. Lin, L. Fu, N. Gedik, and P. Jarillo-Herrero, Observation of the nonlinear hall effect under time-reversal-symmetric conditions, *Nature* **565**, 337 (2018).
- [40] K. Kang, T. Li, E. Sohn, J. Shan, and K. F. Mak, Nonlinear anomalous hall effect in few-layer wte2, *Nature Materials* **18**, 324 (2019).
- [41] Q. Gao, Y. Ren, and Q. Niu, Dc current generation and power feature in strongly driven floquet-bloch systems, *Phys. Rev. Res.* **4**, 013216 (2022).
- [42] H. Dehghani, T. Oka, and A. Mitra, Dissipative floquet topological systems, *Phys. Rev. B* **90**, 195429 (2014).
- [43] H. Dehghani, T. Oka, and A. Mitra, Out-of-equilibrium electrons and the hall conductance of a floquet topological insulator, *Phys. Rev. B* **91**, 155422 (2015).
- [44] K. I. Seetharam, C.-E. Bardyn, N. H. Lindner, M. S. Rudner, and G. Refael, Controlled population of floquet-bloch states via coupling to bose and fermi baths, *Phys. Rev. X* **5**, 041050 (2015).
- [45] T. Iadecola and C. Chamon, Floquet systems coupled to particle reservoirs, *Phys. Rev. B* **91**, 184301 (2015).

- [46] H. Watanabe and Y. Yanase, Chiral photocurrent in parity-violating magnet and enhanced response in topological antiferromagnet, *Phys. Rev. X* **11**, 011001 (2021).
- [47] A. Graf and F. Piéchon, Berry curvature and quantum metric in n -band systems: An eigenprojector approach, *Phys. Rev. B* **104**, 085114 (2021).
- [48] X.-Y. Guo, Z.-Y. Ge, H. Li, Z. Wang, Y.-R. Zhang, P. Song, Z. Xiang, X. Song, Y. Jin, L. Lu, *et al.*, Observation of bloch oscillations and wannier-stark localization on a superconducting quantum processor, *npj Quantum Information* **7**, 51 (2021).
- [49] M. Angeli and A. H. MacDonald, γ valley transition metal dichalcogenide moiré bands, *Proceedings of the National Academy of Sciences* **118**, e2021826118 (2021).
- [50] Y. Cao, V. Fatemi, S. Fang, K. Watanabe, T. Taniguchi, E. Kaxiras, and P. Jarillo-Herrero, Unconventional superconductivity in magic-angle graphene superlattices, *Nature* **556**, 43 (2018).
- [51] Y. Cao, V. Fatemi, A. Demir, S. Fang, S. L. Tomarken, J. Y. Luo, J. D. Sanchez-Yamagishi, K. Watanabe, T. Taniguchi, E. Kaxiras, *et al.*, Correlated insulator behaviour at half-filling in magic-angle graphene superlattices, *Nature* **556**, 80 (2018).
- [52] J. Cai, E. Anderson, C. Wang, X. Zhang, X. Liu, W. Holtzmann, Y. Zhang, F. Fan, T. Taniguchi, K. Watanabe, *et al.*, Signatures of fractional quantum anomalous hall states in twisted mote2, *Nature* **622**, 63 (2023).
- [53] Y. Zeng, Z. Xia, K. Kang, J. Zhu, P. Knüppel, C. Vaswani, K. Watanabe, T. Taniguchi, K. F. Mak, and J. Shan, Thermodynamic evidence of fractional chern insulator in moiré mote2, *Nature* **622**, 69 (2023).
- [54] H. Park, J. Cai, E. Anderson, Y. Zhang, J. Zhu, X. Liu, C. Wang, W. Holtzmann, C. Hu, Z. Liu, *et al.*, Observation of fractionally quantized anomalous hall effect, *Nature* **622**, 74 (2023).
- [55] F. Xu, Z. Sun, T. Jia, C. Liu, C. Xu, C. Li, Y. Gu, K. Watanabe, T. Taniguchi, B. Tong, *et al.*, Observation of integer and fractional quantum anomalous hall effects in twisted bilayer mote 2, *Physical Review X* **13**, 031037 (2023).
- [56] K. Kang, B. Shen, Y. Qiu, Y. Zeng, Z. Xia, K. Watanabe, T. Taniguchi, J. Shan, and K. F. Mak, Evidence of the fractional quantum spin hall effect in moiré mote2, *Nature* **628**, 522 (2024).
- [57] Z. Lu, T. Han, Y. Yao, A. P. Reddy, J. Yang, J. Seo, K. Watanabe, T. Taniguchi, L. Fu, and L. Ju, Fractional quantum anomalous hall effect in multilayer graphene, *Nature* **626**, 759

- (2024).
- [58] J.-X. Yin, B. Lian, and M. Z. Hasan, Topological kagome magnets and superconductors, *Nature* **612**, 647 (2022).
 - [59] Y. Wang, H. Wu, G. T. McCandless, J. Y. Chan, and M. N. Ali, Quantum states and intertwining phases in kagome materials, *Nature Reviews Physics* **5**, 635 (2023).
 - [60] Z. Du, H.-Z. Lu, and X. C. Xie, Nonlinear hall effects, *Nature Reviews Physics* **3**, 744 (2021).
 - [61] D. Ma, A. Arora, G. Vignale, and J. C. W. Song, Anomalous skew-scattering nonlinear hall effect and chiral photocurrents in \mathcal{PT} -symmetric antiferromagnets, *Phys. Rev. Lett.* **131**, 076601 (2023).
 - [62] P. Törmä, Essay: Where can quantum geometry lead us?, *Phys. Rev. Lett.* **131**, 240001 (2023).
 - [63] T. Ozawa and N. Goldman, Probing localization and quantum geometry by spectroscopy, *Phys. Rev. Res.* **1**, 032019 (2019).
 - [64] C.-R. Yi, J. Yu, H. Yuan, R.-H. Jiao, Y.-M. Yang, X. Jiang, J.-Y. Zhang, S. Chen, and J.-W. Pan, Extracting the quantum geometric tensor of an optical raman lattice by bloch-state tomography, *Phys. Rev. Res.* **5**, L032016 (2023).
 - [65] T. Ozawa and N. Goldman, Extracting the quantum metric tensor through periodic driving, *Phys. Rev. B* **97**, 201117 (2018).
 - [66] X. Tan, D.-W. Zhang, Z. Yang, J. Chu, Y.-Q. Zhu, D. Li, X. Yang, S. Song, Z. Han, Z. Li, Y. Dong, H.-F. Yu, H. Yan, S.-L. Zhu, and Y. Yu, Experimental measurement of the quantum metric tensor and related topological phase transition with a superconducting qubit, *Phys. Rev. Lett.* **122**, 210401 (2019).
 - [67] Y. Gao and D. Xiao, Nonreciprocal directional dichroism induced by the quantum metric dipole, *Phys. Rev. Lett.* **122**, 227402 (2019).
 - [68] M. Lysne, M. Schüler, and P. Werner, Quantum optics measurement scheme for quantum geometry and topological invariants, *Phys. Rev. Lett.* **131**, 156901 (2023).